Supplementary Information

Detection of unlabeled nanoplastics within *Daphnia magna* using enhanced darkfield hyperspectral microscopy

*Arav Saherwala[1], Jun-Ray Macairan[1], Emma Geoffroy[1], and Nathalie Tufenkji[1,2] **

[1]Department of Chemical Engineering, McGill University, Montreal, Quebec H3A 0C5, Canada
[2]United Nations University Institute for Water, Environment and Health, Richmond Hill, Ontario, L4B 3P4, Canada

***Corresponding Author**. Phone: (514) 398-2999; E-mail: nathalie.tufenkji@mcgill.ca
This document includes: 29 pages:
23 Figures

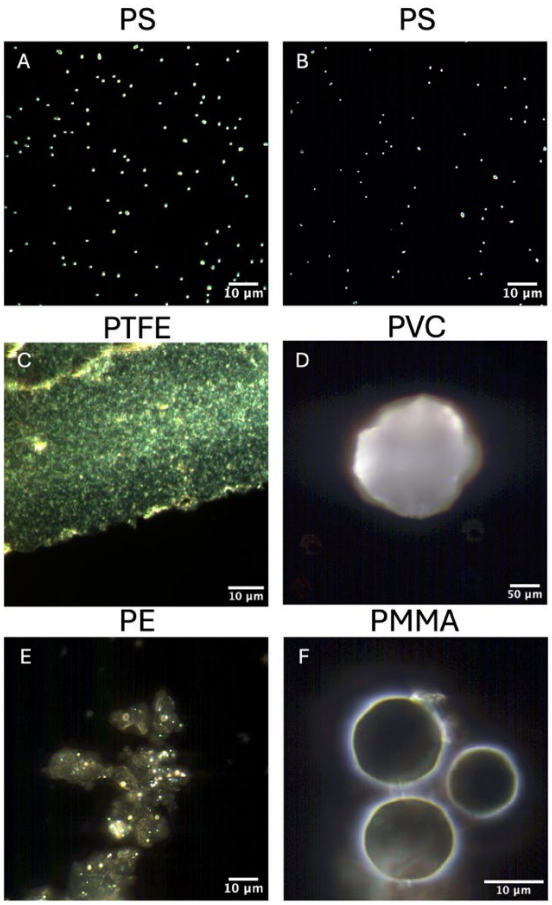

Figure S1. Reference image of plastic microplastics and nanoplastics. Figure S1A is a darkfield image of 750 nm PS particles. Figure S1B is a darkfield image of 500 nm PS particles. Fig S1C is a darkfield image of 200 nm PTFE particles. Figure S1D is a darkfield image of PVC particles with an average size of 63 µm. Figure S1E is a darkfield image of PE particles with an average size of 3 µm. Figure S1F is a darkfield image of 1 to 10 µm PMMA particles. Figure S1C, D, and F were acquired with a half field of view and cropped for visualization purposes. Figure S1A and B brightness and contrast were increased by 40%, and sharpness was increased by 50% for visualization purposes. Figure S1E's sharpness was also increased by 50% for visualization purposes. Original images can be provided upon request.

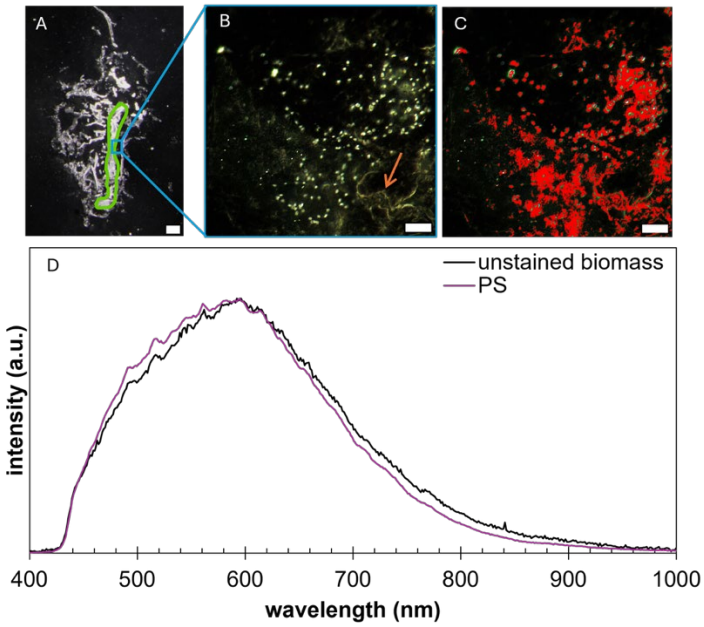

Figure S2. Detection of 750 nm PS within a whole unstained organism. Figure S2A is a 20 µm thick histological slice of a *D. magna* exposed to 750 nm PS at 0.1 ppm. The gut region of the *D. magna* is outlined in green. Figure S2B is a darkfield image acquired on the EDF-HSI microscope. This image is taken in the gut region, as shown by the blue box. The orange arrow points to an area where only biomass is present. Figure S2C shows the Spectral Angle Mapping of the darkfield image taken in Figure S2B. Areas in red indicate where the spectra matched the reference spectra for PS. Figure S2D is the normalized average spectrum of 50 pixels of biomass from Figure S2B, and the normalized average spectrum of 50 pixels of 750 nm PS from Figure S2B. The peak wavelength for unstained biomass is 596 nm, and the peak wavelength for PS within the histological slice is 595 nm. Figure S2A's scale bar represents 200 µm, and in Figures S2B and S2C, the scale bar represents 10 µm. Figure S2A's brightness was decreased by 20%, contrast increased by 40%, and sharpness increased by 50%. Figure S2B and S2C's brightness and contrast were increased by 40%, and the sharpness was increased by 50%. These changes were made for visualization purposes, and original images can be provided upon request.

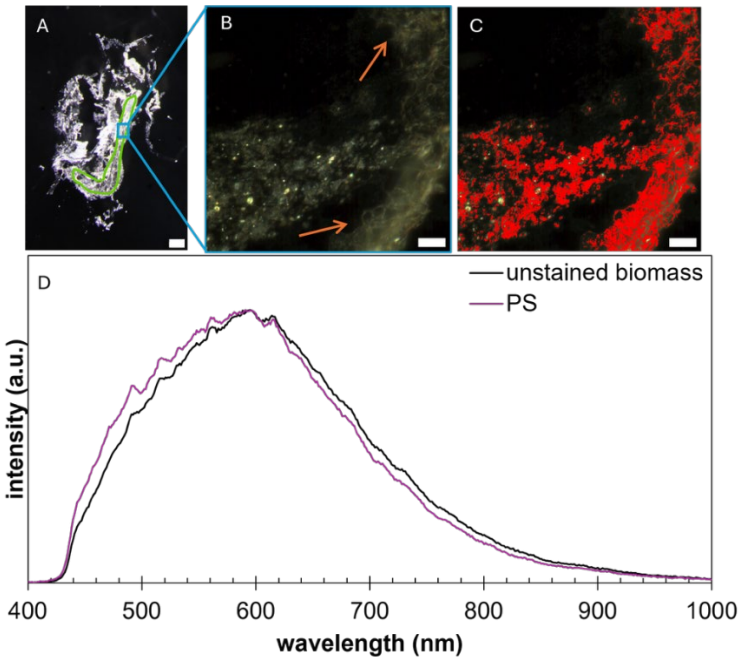

Figure S3. Detection of 750 nm PS within a whole unstained organism. Figure S3A is a 20 µm thick histological slice of a *D. magna* exposed to 750 nm PS at 0.1 ppm. The gut region of the *D. magna* is outlined in green. Figure S3B is a darkfield image acquired on the EDF-HSI microscope. This image is taken in the gut region, as shown by the blue box. The orange arrows point to an area where only biomass is present. Figure S3C shows the Spectral Angle Mapping of the darkfield image taken in Figure S3B. Areas in red indicate where the spectra matched the reference spectra for PS. Figure S3D is the normalized average spectrum of 50 pixels of biomass from Figure S3B and the normalized average spectrum of 50 pixels of 750 nm PS from Figure S3B. The peak wavelength for unstained biomass is 595 nm, and the peak wavelength for PS within the histological slice is 591 nm. Figure S3A's contrast was increased by 40% and sharpness by 50% for visualization purposes. Original images can be provided upon request. Figure S3A's scale bar represents 200 µm, and in Figure S3B and S3C, the scale bar represents 10 µm.

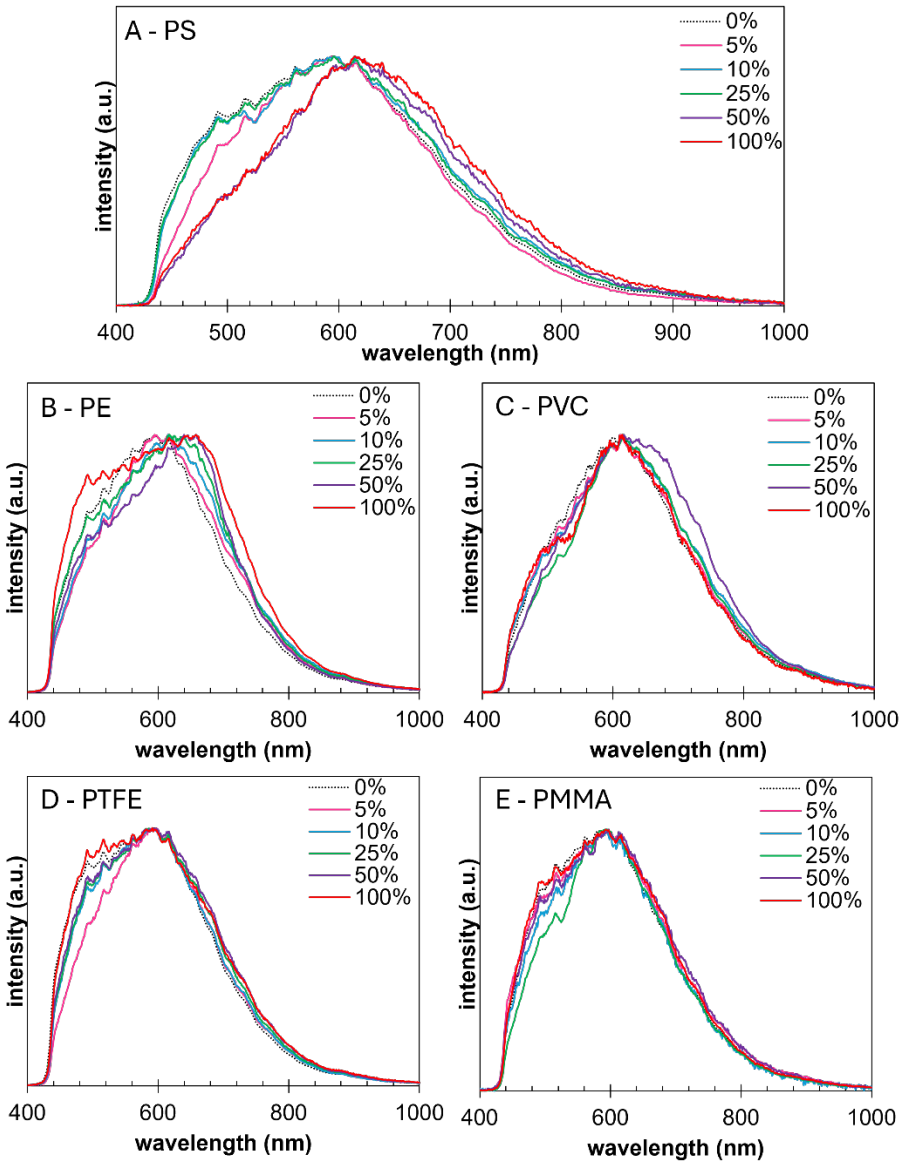

Figure S4. Each graph shows the average normalized spectrum of 50 pixels of the respective polymer type after being stained with different concentrations of H&E stain. Figure S4 A, B, C, D, and E show PS, PE, PVC, PTFE, and PMMA spectra, respectively, after staining with 5%, 10%, 25%, 50%, and 100% H&E stains. The 0% stain in each graph corresponds to the reference spectrum of unstained plastic.

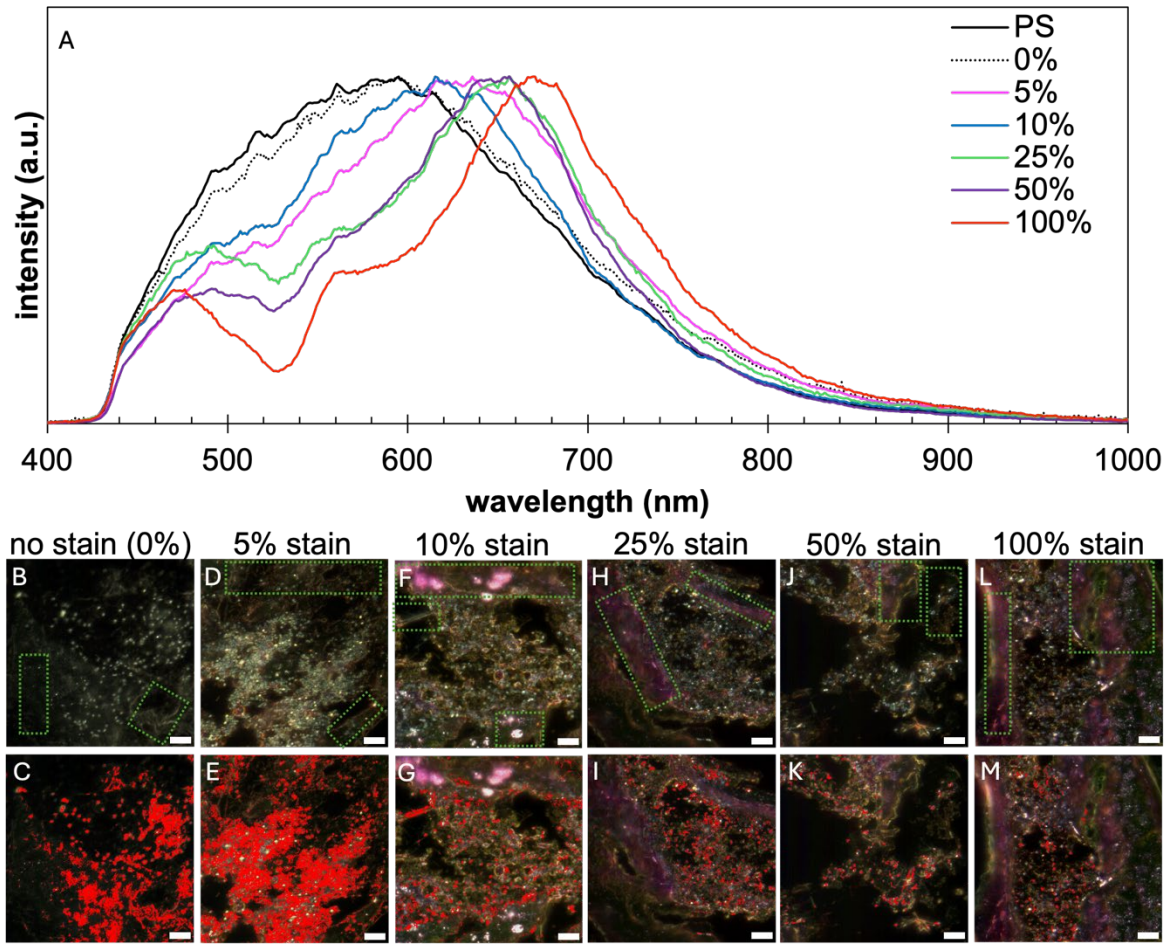

Figure S5. Second replicate of H&E staining of histological slices at different stain concentrations. All *D. magna* were exposed to 750 nm PS at 0.1 ppm, and all histological slices were 20 µm thick. Figure S5A presents the normalized average spectra of 50 pixels of biomass from each histological slice from Figure S5B, D, F, H, J, and L (scale bar: 10 µm). The spectrum of reference PS in a histological slice is also presented in Figure S5A (solid black). Figure S5B is unstained, and the corresponding Spectral Angle Mapping image is in Figure S5C, where red parts indicate mapped areas (*i.e.*, spectra of the red areas match with the PS reference library). The remaining panels show images of *D. magna* stained with different concentrations of stain: Figure S5D-E have been stained with 5% H&E, Figure S5F-G have been stained with 10% H&E, Figure S5H-I have been stained with 25% H&E, Figure S5J-K have been stained with 50% H&E, and Figure S5L-M have been stained with 100% H&E. Figure S5C, E, G, I, K and M are the Spectral Angle Mapping images where red parts indicate mapped areas (scale bar: 10 µm). Green boxes on Figure S5B, D, F, H, J, and L indicate where the biomass spectra for each staining concentration were taken from.

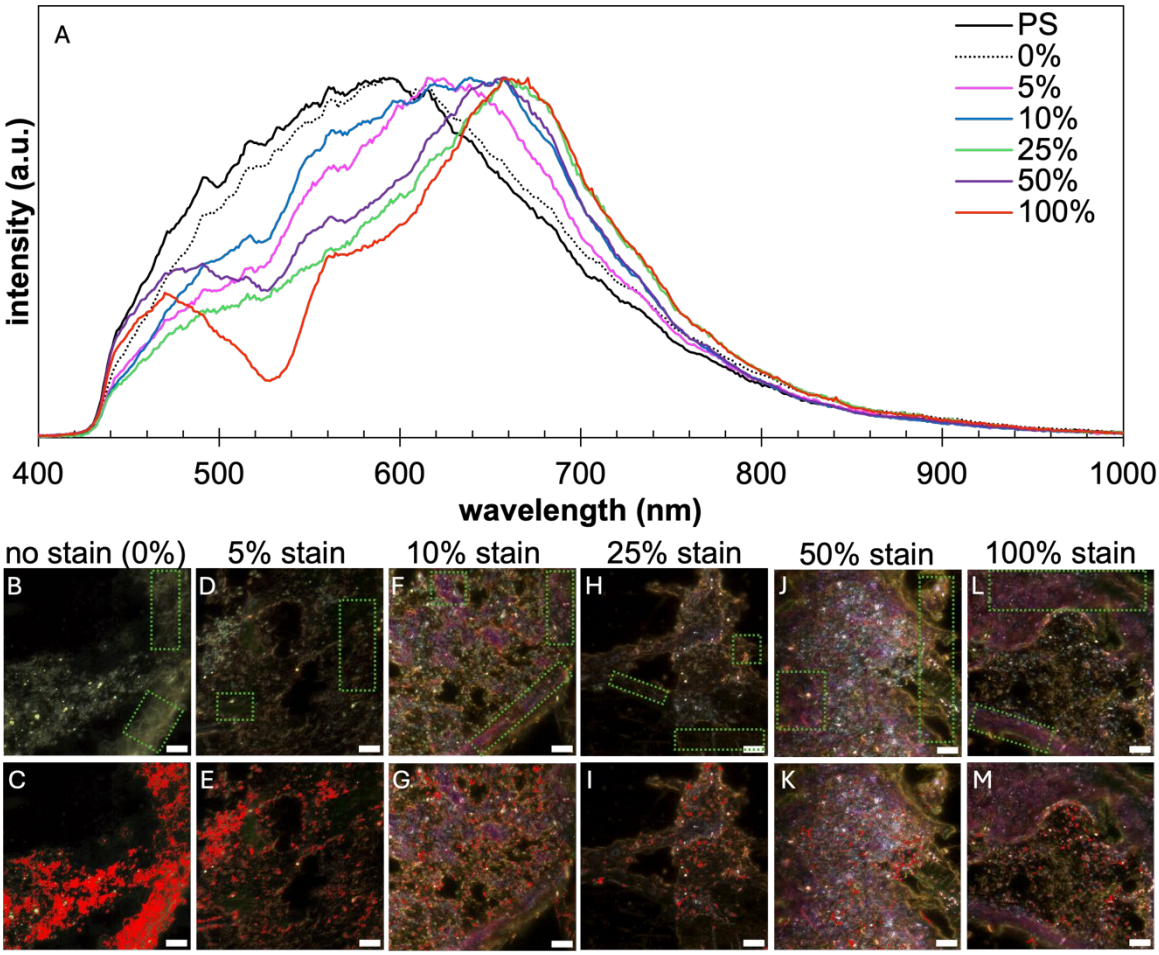

Figure S6. Third replicate of H&E staining of histological slices at different stain concentrations. All *D. magna* were exposed to 750 nm PS at 0.1 ppm, and all histological slices were 20 µm thick. Figure S6A presents the normalized average spectra of 50 pixels of biomass from each histological slice from Figure S6B, D, F, H, J, and L (scale bar: 10 µm). The spectrum of reference PS in a histological slice is also presented in Figure S6A (solid black). Figure S6B is unstained, and the corresponding Spectral Angle Mapping image is in Figure S6C, where red parts indicate mapped areas (*i.e.*, spectra of the red areas match with the PS reference library). The remaining panels show images of *D. magna* stained with different concentrations of stain: Figure S6D-E have been stained with 5% H&E, Figure S6F-G have been stained with 10% H&E, Figure S6H-I have been stained with 25% H&E, Figure S6J-K have been stained with 50% H&E, and Figure S6L-M have been stained with 100% H&E. Figure S6C, E, G, I, K and M are the Spectral Angle Mapping images where red parts indicate mapped areas (scale bar: 10 µm). Green boxes on Figure S6B, D, F, H, J, and L indicate where the biomass spectra for each staining concentration were taken from.

Table S1. Peak wavelength of 50 pixels of biomass for each H&E staining concentration. The average peak wavelength is the average across the three replicates, and its standard deviation.

H&E staining concentration	Peak wavelength replicate 1 (nm)	Peak wavelength replicate 2 (nm)	Peak wavelength replicate 3 (nm)	Average peak wavelength (nm)
0%	597.38	596.10	594.83	596.10 ± 1.27
5%	615.24	635.77	615.24	622.08 ± 11.85
10%	638.34	615.24	639.63	631.07 ± 13.73
25%	655.12	656.42	657.71	656.42 ± 1.29
50%	683.71	656.42	657.71	665.95 ± 15.40
100%	657.71	670.69	670.69	666.36 ± 7.49

Table S2. Statistical analysis on the Spectral Angle Mapping tool at different H&E staining concentrations.

H&E staining concentration:	0%	5%	10%	25%	50%	100%
Percent true positive (correctly detected particle)	96.26 ± 4.12%	99.27 ± 0.64%	87.71 ± 8.47%	94.38 ± 3.35%	87.45 ± 6.32%	89.45 ± 0.95%
Percent false negative (particle present but not detected)	3.74 ± 4.12 %	0.73 ± 0.64%	12.29 ± 8.47%	5.62 ± 3.35%	12.55 ± 6.32%	10.55 ± 0.95%
Percent false positive (detected but no particle present)	too high to count	too high to count	12.33 ± 12.33%	6.88 ± 3.04%	7.68 ± 2.35%	5.53 ± 3.92%

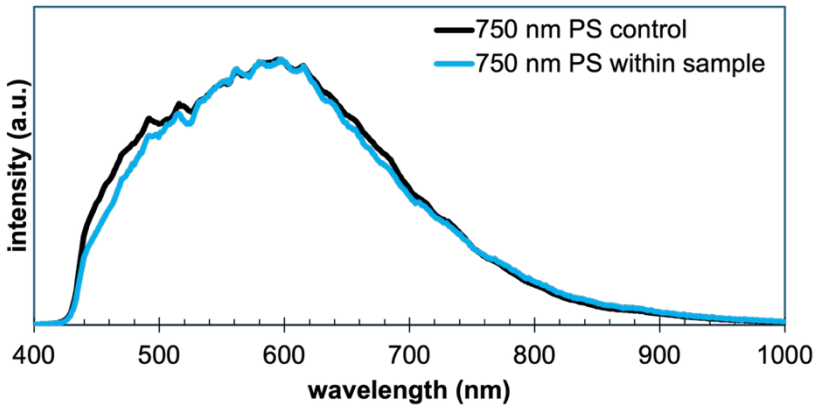

Figure S7. The average spectrum of a reference PS is compared with that of PS within a histological slice stained with 25% H&E. The average peak wavelength of reference PS particles is 595 nm, and the average peak wavelength of PS particles within the histological slice is 597 nm. The average normalized spectrum for 750 nm PS control and within a sample were calculated from 50 pixels.

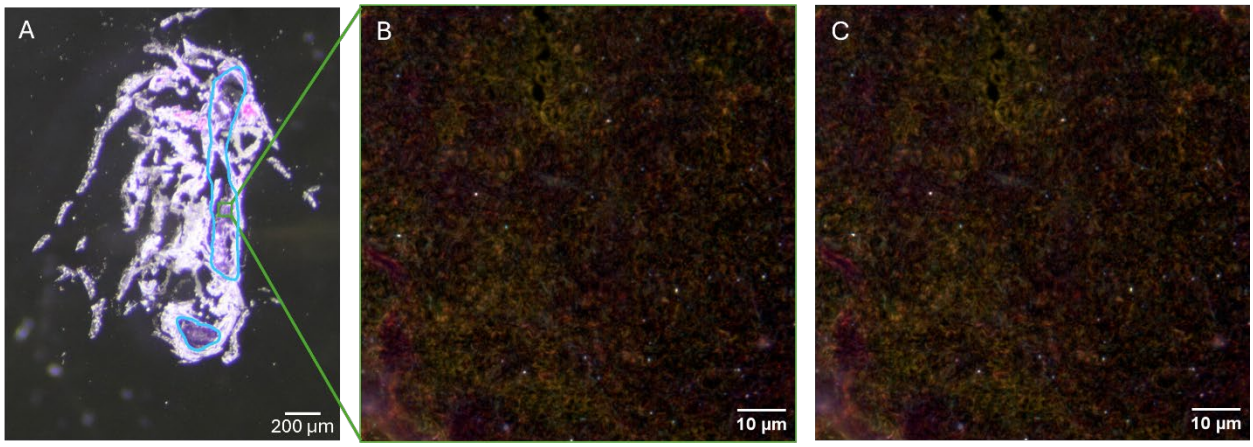

Figure S8. A control *D. magna*'s gut was imaged. Figure S8A is a darkfield image of a histological slice of the control sample. The gut region is outlined in blue. Figure S8B is a darkfield image acquired on the EDF-HSI microscope of an area in the gut. Figure S8C is the corresponding mapped image, where it is evident that the Spectral Angle Mapping tool did not detect any plastic particles within the control sample.

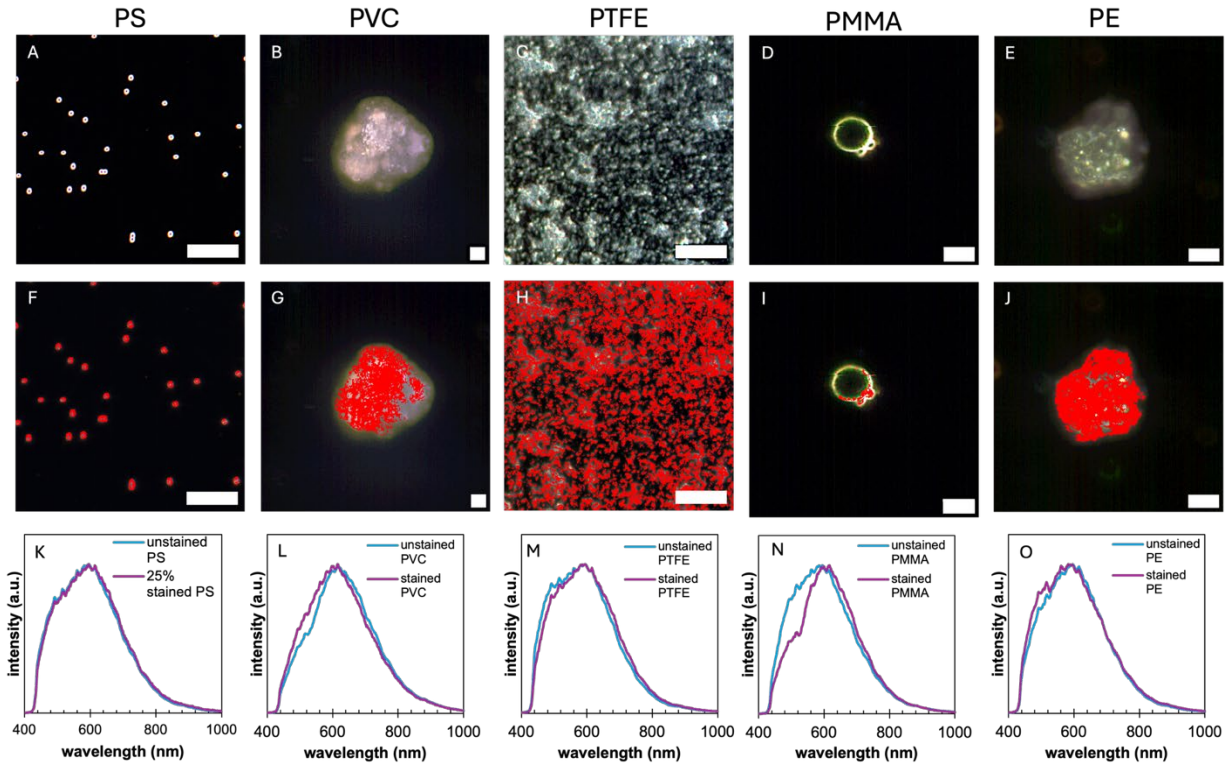

Figure S9. Different plastic types stained with 25% H&E. Figure S9 A, B, C, D, and E are the darkfield images of 25% H&E stained 750 nm PS, 63 µm PVC, 200 nm PTFE, 1-10 µm PMMA, and 3 µm PE particles, respectively. Figure S9F, G, H, I, and J are the corresponding mapped images for each plastic type using the Spectral Angle Mapping tool, indicating that all particles were detected. This demonstrates that different plastic particles are not affected by the staining protocol and remain unlabeled. Figure S9K, L, M, N, and O show the average spectrum of unstained and stained particles for each plastic type. Here, the shape of the graph and the peak wavelength remain very similar before and after staining, except for PMMA, which has a shallower spectrum from 400 nm to 616 nm, resulting in the incomplete mapping of PMMA particles seen in Figure S9I. The peak wavelength before staining of PS is 595 nm, PVC is 615 nm, PTFE is 595 nm, PMMA is 594 nm, and PE is 596 nm. The reference spectra of the plastics (i.e. unstained plastic spectra) have been reused in all replicates (Figures S10 and S11). The peak wavelength after staining for PS is 596 nm, PVC is 615 nm, PTFE is 595 nm, PMMA is 595 nm, and PE is 594 nm. Figure S9B, C, E, F, G, H, and J were acquired with a half field of view and cropped for visualization purposes. Figure S9A and D's brightness and contrast were increased by 40% and sharpness increased by 50%. Figure S9E's brightness was increased by 20%, contrast was increased by 40%, and sharpness increased by 50%. Figure S9B sharpness was increased by 50%. Figure S9C's sharpness was increased by 50% and brightness by 40%. These changes were made for visualization purposes, and raw images can be provided upon request. Figure S9B and S9G's scale bar represents 30 µm, and the remaining images' scale bar represents 10 µm.

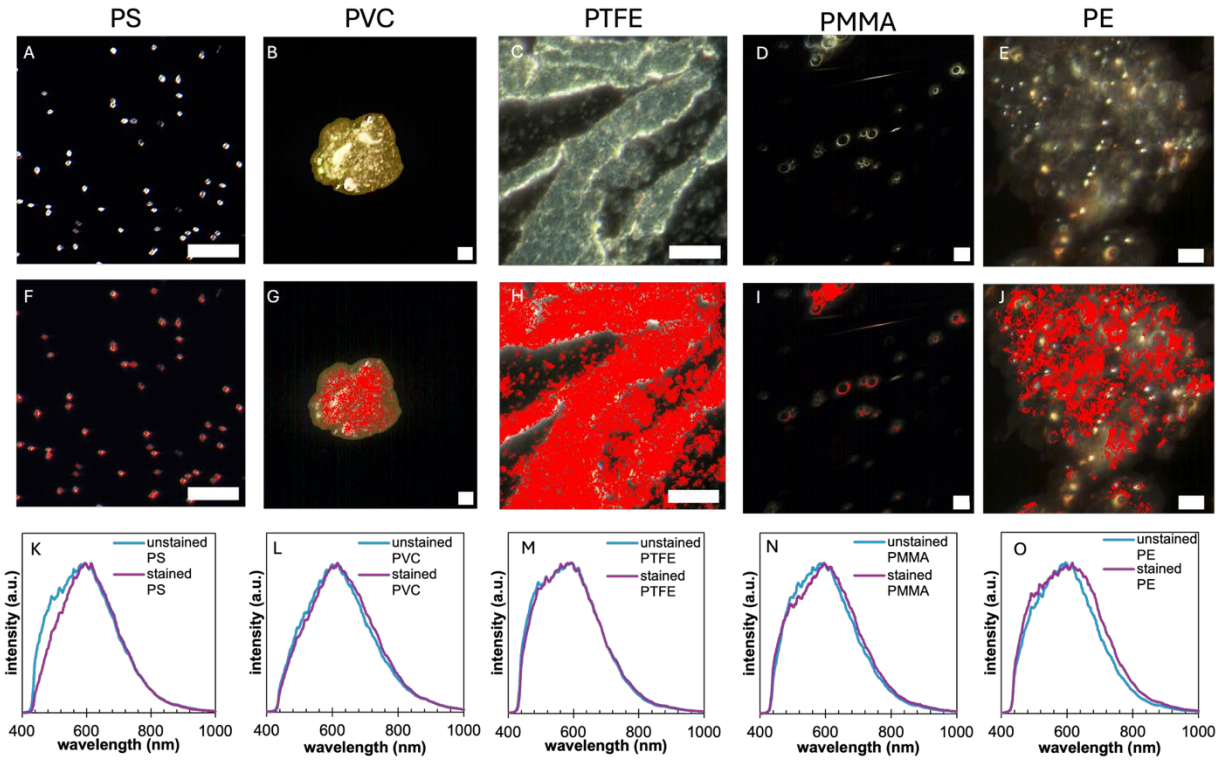

Figure S10. Second replicate of different plastic types stained with 25% H&E. Figure S10A, B, C, D, and E are the darkfield images of 25% H&E stained 750 nm PS, 63 µm PVC, 200 nm PTFE, 1-10 µm PMMA, and 3 µm PE particles, respectively. Figure S10F, G, H, I, and J are the corresponding mapped images for each plastic type using the Spectral Angle Mapping tool, indicating that all particles were detected. This demonstrates that different plastic particles are not affected by the staining protocol and remain unlabeled. Figure S10K, L, M, N, and O show the average spectrum of unstained and stained particles for each plastic type. The peak wavelength before staining of PS is 595 nm, PVC is 615 nm, PTFE is 595 nm, PMMA is 594 nm, and PE is 596 nm. The reference spectra of the plastics (i.e. unstained plastic spectra) have been reused in all replicates (Figures S9 and S11). The peak wavelength after staining for PS is 596 nm, PVC is 617 nm, PTFE is 591 nm, PMMA is 596 nm, and PE is 617 nm. Figure S10A, C, E, F, H, and J were acquired with a half field of view and cropped for visualization purposes. Figure S10A and D's brightness and contrast were increased by 40% and sharpness increased by 50%. Figure S10B's brightness was increased by 20%, contrast was increased by 40%, and sharpness was increased by 50%. These changes were made for visualization purposes, and raw images can be provided upon request. Figure S10B and S10G's scale bar represents 30 µm, and the remaining images' scale bar represents 10 µm.

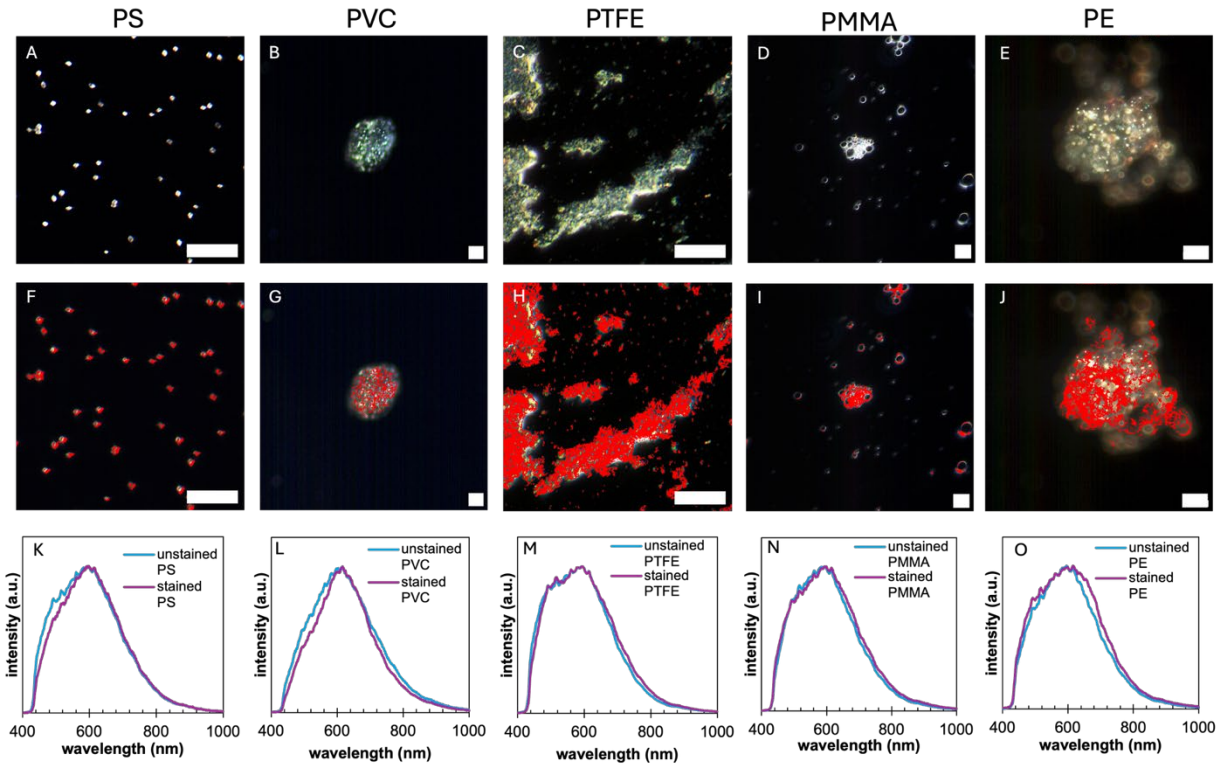

Figure S11. Third replicate of different plastic types stained with 25% H&E. Figure S11A, B, C, D, and E are the darkfield images of 25% H&E stained 750 nm PS, 63 µm PVC, 200 nm PTFE, 1-10 µm PMMA, and 3 µm PE particles, respectively. Figure S11F, G, H, I, and J are the corresponding mapped images for each plastic type using the Spectral Angle Mapping tool, indicating that all particles were detected. This demonstrates that different plastic particles are not affected by the staining protocol and remain unlabeled. Figure S11K, L, M, N, and O show the average spectrum of unstained and stained particles for each plastic type. The peak wavelength before staining of PS is 595 nm, PVC is 615 nm, PTFE is 595 nm, PMMA is 594 nm, and PE is 596 nm. The reference spectra of the plastics (i.e. unstained plastic spectra) have been reused in all replicates (Figures S9 and S10). The peak wavelength after staining for PS is 596 nm, PVC is 617 nm, PTFE is 595 nm, PMMA is 596 nm, and PE is 615 nm. Figure S11A, B, C, F, G, and H were acquired with a half field of view and cropped for visualization purposes. Figure S11A's brightness and contrast were increased by 40% and sharpness increased by 50%. Figure S11B and C's contrast was increased by 40% and sharpness was increased by 50%. Figure S11D's brightness was increased by 20%, contrast was increased by 40%, and sharpness was increased by 50%. These changes were made for visualization purposes, and raw images can be provided upon request. Figure S11B and S11G's scale bar represents 30 µm, and the remaining images' scale bar represents 10 µm.

Validating Spectral Angle Mapping. An optical photothermal infrared (O-PTIR) microscope was used to validate the Spectral Angle Mapping tool's detection of PE, PTFE, PVC, PMMA, and PS. The O-PTIR microscope model is a mIRage-R from Photothermal Spectroscopy Corporation. The microscope is fitted with an IR pump beam (MIRcat 2400, Daylight) and a 532 nm probe laser. The IR has a range between 1800–800 cm^{-1} and 3000–2650 cm^{-1}. An Avalanche Photodiode is also used to improve the sensitivity. In general, the O-PTIR measures the photothermal response of the sample by using a pump-probe mechanism. O-PTIR validation was completed for PTFE, PE, PVC, and PMMA using the same slices seen in Figure 4. However, for PS, the small size of the particles along with the low concentration makes it difficult to obtain PS spectra using O-PTIR. Hence, *D. magna* was exposed to 1 ppm of 750 nm PS, which allowed for better IR acquisition using O-PTIR. In **Figure S14**, it can be observed that the Spectral Angle Mapping tool correctly detected PS, as shown by the IR spectra in **Figure S14E**. This validation also demonstrates how the method in this study can be used in conjunction with other characterization techniques.

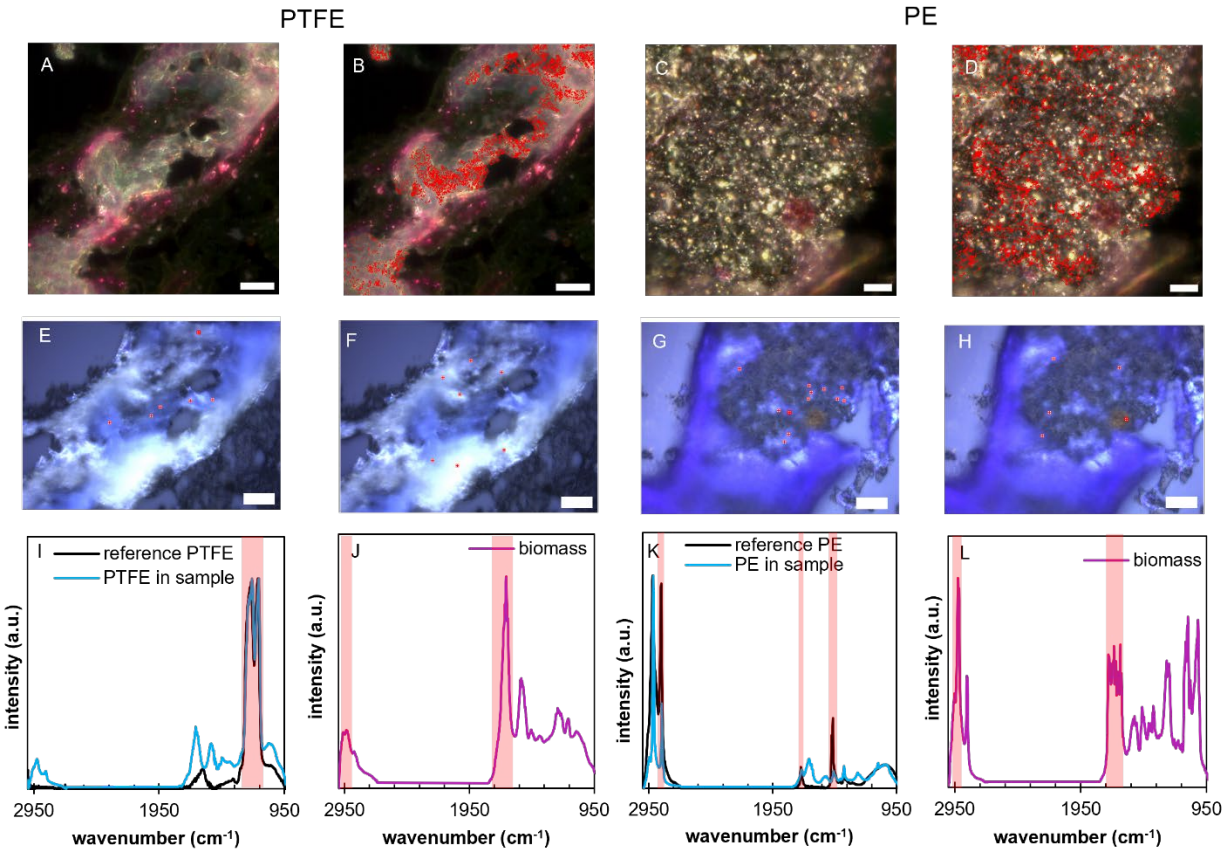

Figure S12. Figure S12A is the darkfield image of a section of the gut from a *D. magna* exposed to 0.1 ppm of PTFE. Figure S12B is the corresponding hyperspectral image showing the detected PTFE particles in red. Figure S12E is an image captured on the O-PTIR microscope, where the red crosshairs indicate where IR signals were acquired and corresponded to PTFE. Figure S12I is the average IR signal from the points shown in Figure S12E. The average IR spectrum matches that of reference PTFE, shown by the black spectra. The red highlights indicate the characteristic

peak wavenumbers for PTFE (1209 cm^{-1}, and 1151 cm^{-1}). Figure S12C is the darkfield image of a *D. magna* exposed to 1 ppm of PE. Figure S12D is the corresponding hyperspectral image showing the detected PE particles in red. Figure S12G is an image captured on the O-PTIR microscope, where the red crosshairs indicate where IR signals were acquired and correspond to PE. Figure S12K is the average IR signal from the points shown in Figure S12G. The average IR acquired on the O-PTIR matches that of reference PE, shown by the black spectra. The red highlights indicate the characteristic peak wavenumber for PE (2850 cm^{-1}, 1720 cm^{-1}, and 1476 cm^{-1}). The same field of view was imaged using the EDF-HSI and O-PTIR microscopes. The red crosshairs in Figure S12F and S12H indicate where IR signals were acquired that correspond to biomass. In Figure S12J and S12L, the red highlight indicates characteristic peak wavenumbers for biomass (2925 cm^{-1} and 1746 cm^{-1}).[1] Figure S12A and B's scale bar represents 10 μm, and Figures S12C-H's scale bar represents 20 μm.

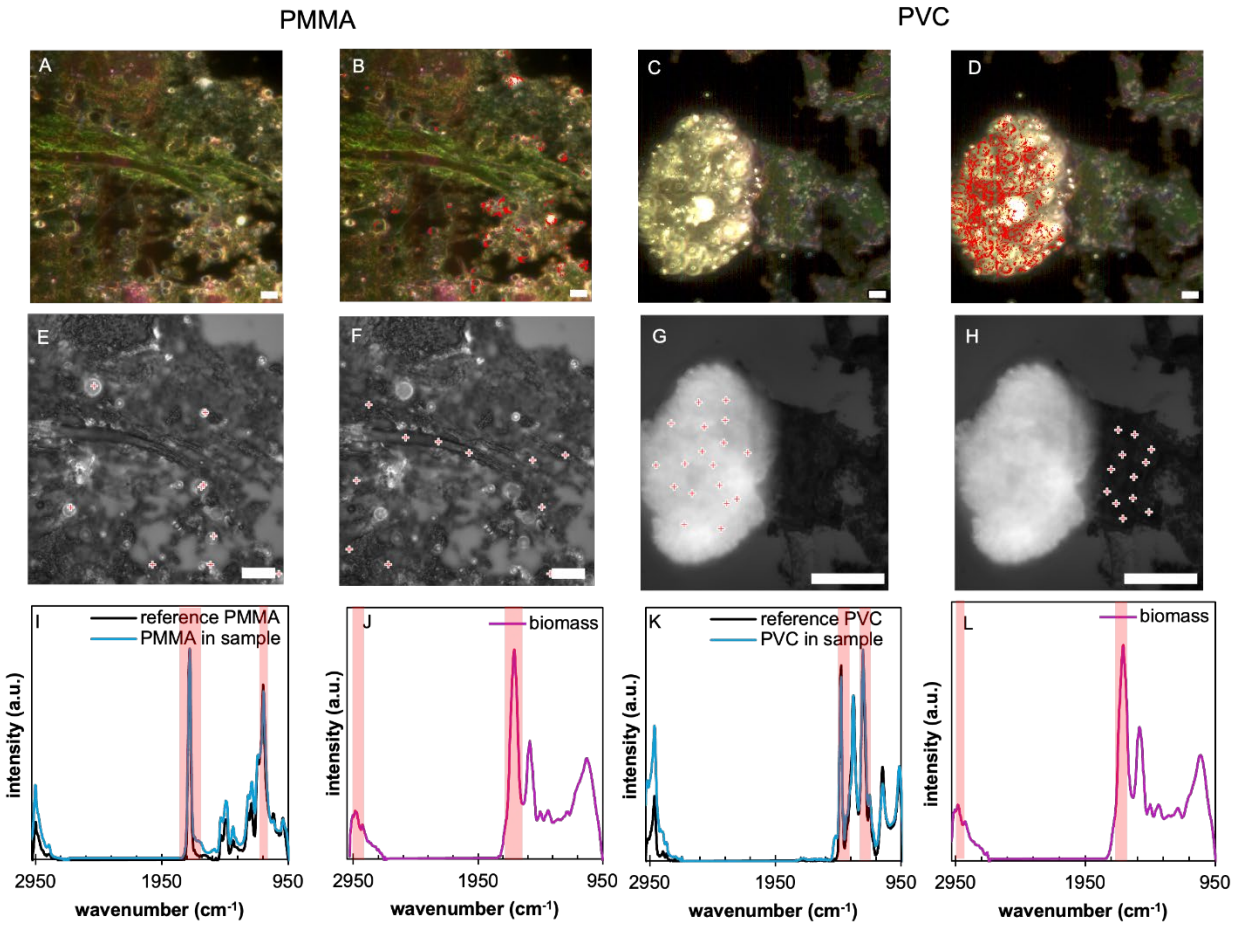

Figure S13. Figure S13A is the darkfield image of a section of the gut from a *D. magna* exposed to PMMA. Figure S13B is the corresponding hyperspectral image showing the detected PMMA particles in red. Figure S13E is an image captured on the O-PTIR microscope, where the red crosshairs indicate where IR signals were acquired and corresponded to PMMA. Figure S13I is the average IR signal from 12 points shown in Figure S13E. The average IR spectrum matches that of reference PMMA, shown by the black spectra. The red highlights indicate the characteristic peak wavenumbers for PMMA (1725 cm^{-1} and 1151 cm^{-1}).[1] Figure S13C is the darkfield image of a *D. magna* exposed to PVC. Figure S13D is the corresponding hyperspectral image showing the detected PVC in red. Figure S13G is an image captured on the O-PTIR microscope, where the red crosshairs indicate where IR signals were acquired and correspond to PVC. Figure S13K is the average IR signal from 18 points shown in Figure S13G. The average IR spectrum acquired on the O-PTIR matches that of reference PVC, shown by the black spectra. The red highlights indicate the characteristic peak wavenumber for PVC (1427 cm^{-1} and 1255 cm^{-1}). The same field of view was imaged using the EDF-HSI and O-PTIR microscopes. The red crosshairs in Figure S13F and S13H indicate where IR signals were acquired that correspond to biomass. In Figure S13J and S13L, the red highlight indicates characteristic peak wavenumbers for biomass (2925 cm^{-1} and 1746 cm^{-1}).[1] Figure S13A-D's scale bar represents 10 μm, and Figures S13E-H's scale bar represents 20 μm.

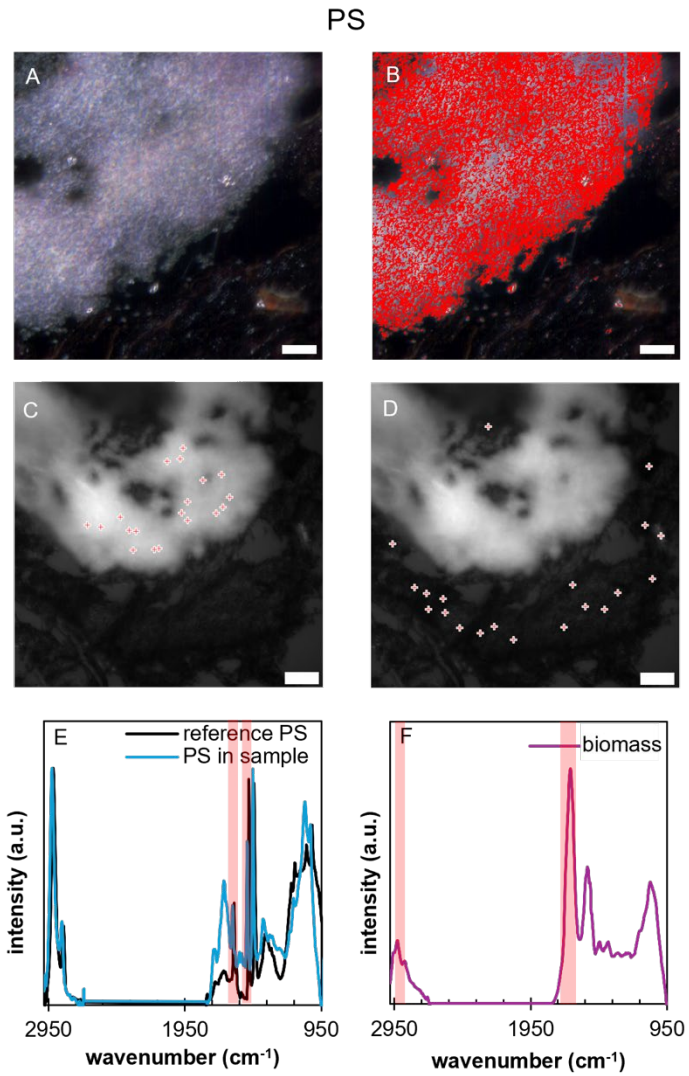

Figure S14. Figure S14A is the darkfield image of a section of the gut from a *D. magna* exposed to 1 ppm of 750 nm PS. Figure S14B is the corresponding hyperspectral image showing the detected PS particles in red. Figure S14C is an image captured on the O-PTIR microscope, where the red crosshairs indicate where IR signals were acquired and corresponded to PS. Figure S14E is the average IR signal from 19 points shown in Figure S14C. The average IR spectrum matches that of reference PS, shown by the black spectra. The red highlights indicate the characteristic peak wavenumbers for PS (1492 cm^{-1} and 1601 cm^{-1}).[1] The same field of view was imaged using the EDF-HSI and O-PTIR microscopes. The red crosshairs in Figure S14D indicate where IR signals were acquired from 20 points that correspond to biomass. In Figure S14F, the red highlight indicates characteristic peak wavenumbers for biomass (2925 cm^{-1} and 1746 cm^{-1}).[1] Figure S14A and B's scale bar represents 10 μm, and Figures S14C and D's scale bar represents 20 μm.

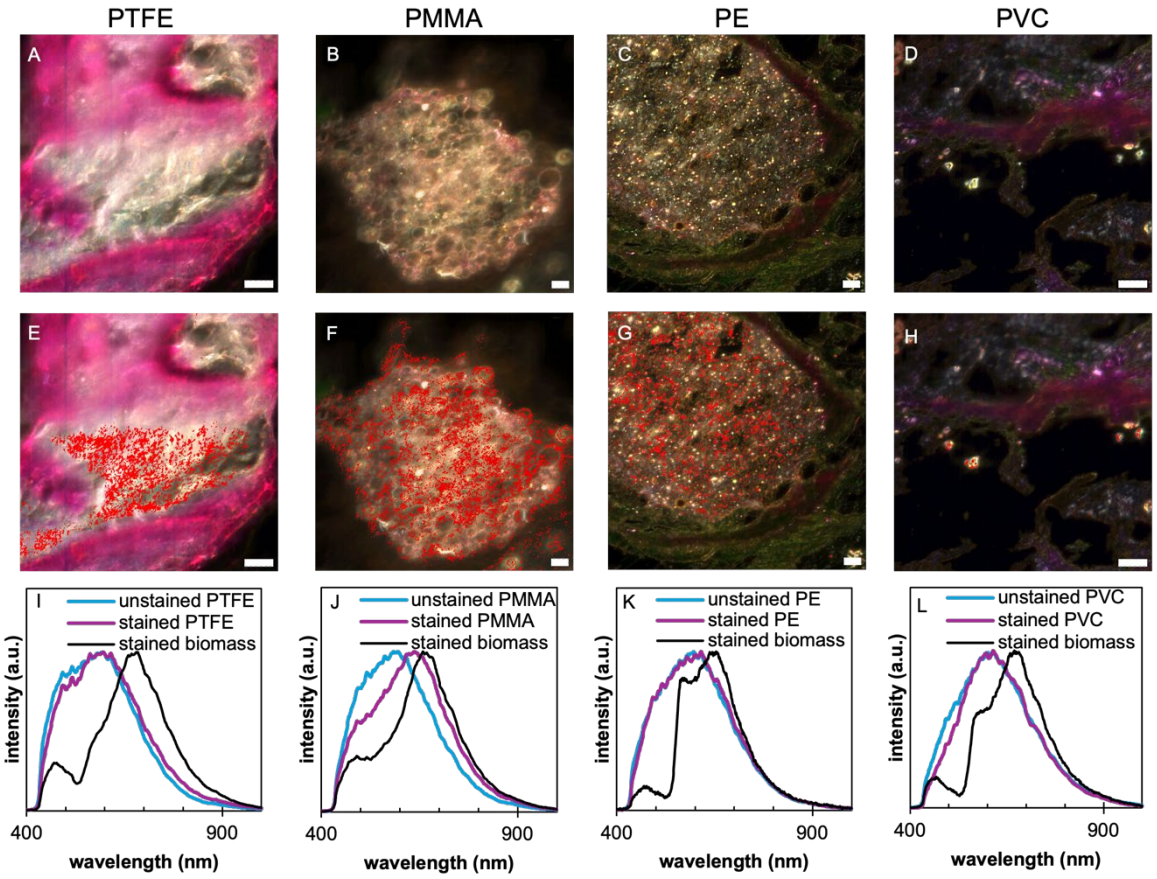

Figure S15. Second replicate of detecting different polymers in *D. magna.* The darkfield images of *D. magna* exposed to (A) 0.1 ppm of 200 nm PTFE, (B) 1 ppm of 1-10 µm PMMA, (C) 1 ppm of 3 µm PE, and (D) 10 ppm of 63 µm PVC are shown in the first row. In the second row, corresponding red pixels matched by the Spectral Angle Mapping Tool for (E) PTFE, (F) PMMA, (G) PE, and (H) PVC are shown. The last row shows the control and stained polymer spectra of (I) PTFE, (J) PMMA, (K) PE, and (L) PVC. The peak wavelength of PTFE, PMMA, PE, and PVC within the sample is 594 nm, 638 nm, 615 nm, and 615 nm, respectively, whereas the control (unstained) PTFE, PMMA, PE, and PVC is 595 nm, 594 nm, 596 nm, and 615 nm, respectively. The reference spectrum for the unstained plastic particles (blue curve) is the same in all replicates. Scale bar in all images represent 10 µm. Figure S15A and S15E's brightness and contrast have been increased by 20%. Figure S15C and S15G's brightness was increased by 20%. Figure S15D and S15H's brightness was increased by 20% and sharpness was increased by 50%. These changes were made for visualization purposes, and original images can be provided upon request.

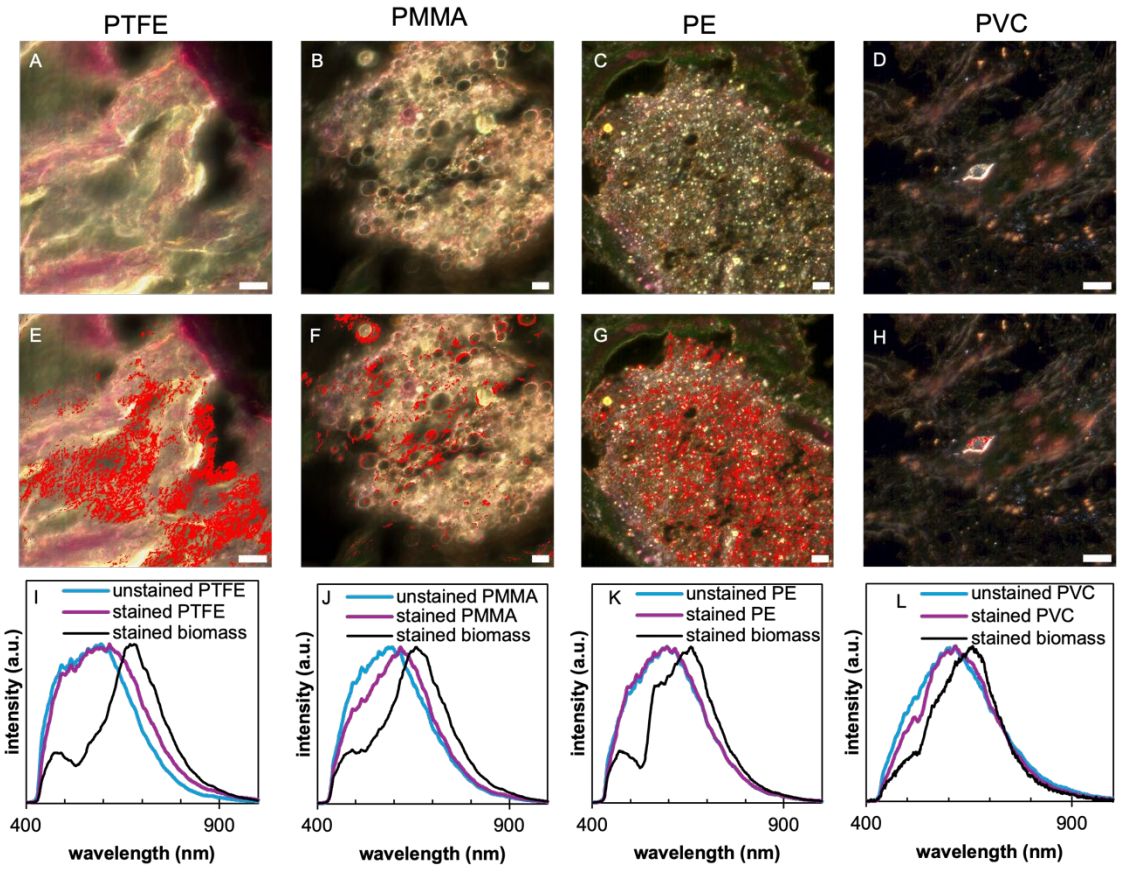

Figure S16. Third replicate of detecting different polymers in *D. magna.* The darkfield images of *D. magna* exposed to (A) 0.1 ppm of 200 nm PTFE, (B) 1 ppm of 1-10 µm PMMA, (C) 1 ppm of 3 µm PE, and (D) 10 ppm of 63 µm PVC are shown in the first row. In the second row, corresponding red pixels matched by the Spectral Angle Mapping Tool for (E) PTFE, (F) PMMA, (G) PE, and (H) PVC are shown. The last row shows the control and stained polymer spectra of (I) PTFE, (J) PMMA, (K) PE, and (L) PVC. The peak wavelength of PTFE, PMMA, PE, and PVC within the sample is 615 nm, 617 nm, 596 nm, and 617 nm, respectively, whereas the control (unstained) PTFE, PMMA, PE, and PVC is 595 nm, 594 nm, 596 nm, and 615 nm, respectively. The reference spectrum for the unstained plastic particles (blue curve) is the same in all replicates. Scale bar in all images represent 10 µm. Figure S16C and S16E's brightness and contrast have been increased by 20%. Figure S16C and S16G's brightness was increased by 20%. Figure S16D and S16H's brightness was increased by 40%. These changes were made for visualization purposes, and original images can be provided upon request.

Vertical Image Stacks. The 20 µm thick histological slices result in some areas of acquired darkfield images to be more in-focus than other parts, as evident in **Figure S17B**, where particles in focus are identified with a green arrow. The remaining particles are visually observed but are distorted due to the scattering of light. This results in the Spectral Angle Mapping tool identifying more areas as plastic, as evident in **Figure S17E**. To address this, images were acquired throughout the histological slice's z-axis, creating a vertical stack of images, shown in **Figure S17B-D**. Acquiring images at various focal depths is helpful in visually confirming particles that are present in those areas. **Figure S17F-G** confirm that the Spectral Angle Mapping algorithm correctly detected nanoplastics; the green arrows in **Figure S17C** and **S17D** point to particles that were not in focus in **Figure S17B**. An additional example of a vertical stack can be observed in **Figure S18**.

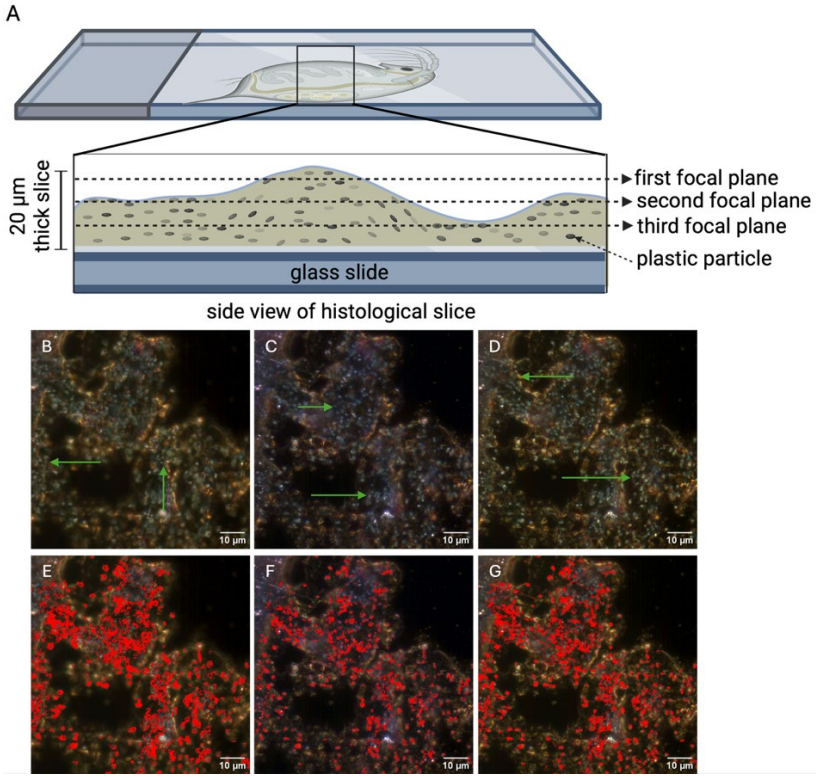

Figure S17. Vertical stack of *D. magna* exposed to 750 nm PS particles at a concentration of 0.1 ppm. Histological slices were stained with 25% H&E staining. Figure S17A is a diagram showing the side view of a histological slice and shows an example of different focal planes in a histological slice. Figure S17B is the first image in the vertical stack, where the green arrows point to a few particles that are in focus compared to the other particles. Figure S17E is the corresponding Spectral Angle Mapping image, where red parts indicate the detection of the PS particles. Figure S17C is the second image in the stack, where the distorted particles from Figure S17B are in focus, shown by the green arrows. Figure S17F is the corresponding Spectral Angle Mapping image, where red parts indicate the detection of the PS particles. Figure S17D is the last image in the vertical stack, where new particles in focus are shown with a green arrow. Figure S17G is the corresponding Spectral Angle Mapping image, where red parts indicate the detection

of the PS particles. Figure S17A was created in BioRender. Saherwala, A. (2025) https://BioRender.com/0zwx9ju

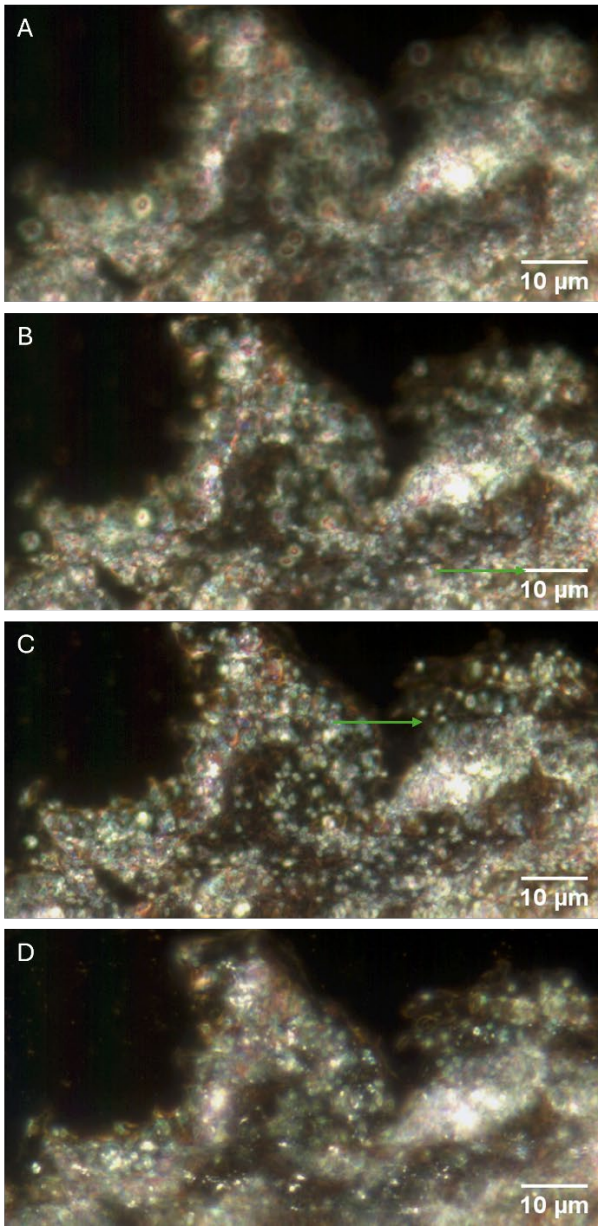

Figure S18. Images at various focal depths to acquire a "z-stack." Figure S18A is the first image in the stack where everything is out of focus. Figure S18B and S18C focus on more particles, as shown by a green arrow on each respective image. Figure S18D is the last image, where most of the particles are out of focus. The *D. magna* was exposed to 750 nm PS at a concentration of 0.1 ppm. The darkfield images were captured with a half-field of view.

In future work, thinner histological slices can be acquired to reduce the number of particles that are out of focus. Another advantage of using thinner histological slices (i.e. 10 µm) is that this can enhance particle detection in a sample by minimizing biomass interference. The thinner histological slice results in less biomass being present on a slice and thus less z-axis variability in a slice. This can be observed in **Figure S19**, where a single image captures all particles in focus within the field of view. These factors can result in better particle detection as biomass interference would be reduced. However, slices that are too thin may compromise the structural integrity of the organism and disrupt particle localization. For example, in **Figure S20A**, it can be observed that the structural integrity of the sample is disrupted, and less biomass is present compared to **Figure S20B**. This is due to the thinner cryotome slice, which makes it challenging to transfer onto a glass slide without disturbing the sample. Thus, while thinner slices may improve particle mapping and detection, they may not be suitable for researchers interested in the spatial distribution of particles within the organism. In such cases, 20 µm thick slices should be used.

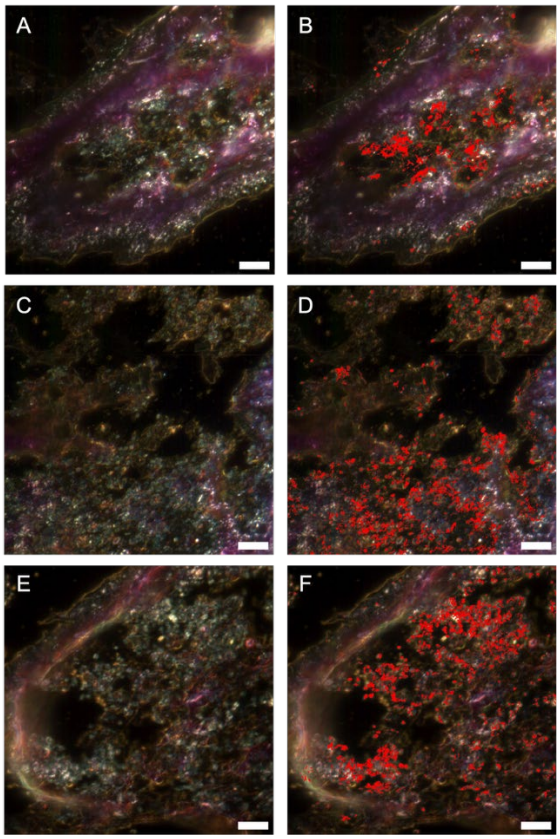

Figure S19. Particle detection in 10 µm thick histological slices. Figure S19A, C and E are three separate slices of *D. magna* exposed to 750 nm PS particles at 0.1 ppm and stained with 25% H&E stain. Figure S19B, D and F are the corresponding mapped images.

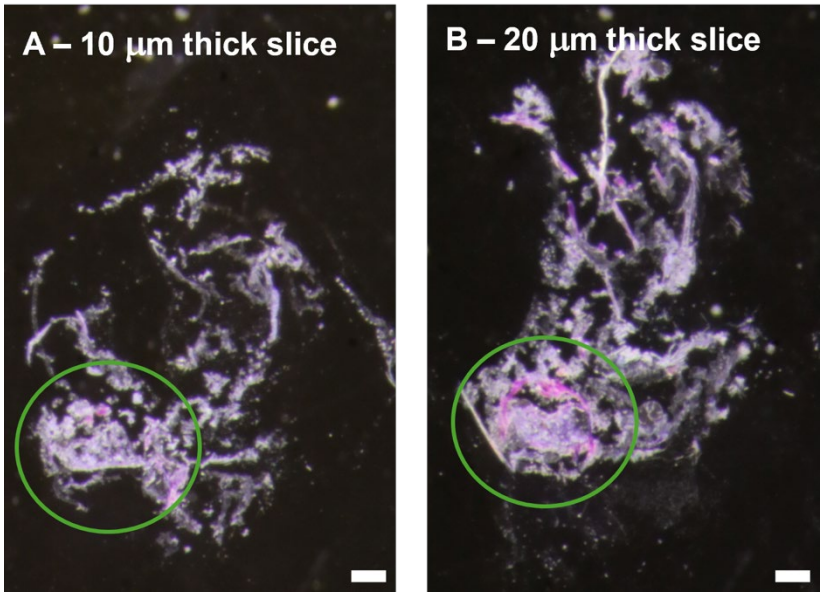

Figure S20. Comparing structure of *D. magna* in 10 µm thick slice versus 20 µm thick slice. The *D. magna* was exposed to 750 nm PS at 0.1 ppm and stained with 25% H&E. Figure S20A and B are slices from the same *D. magna* that were acquired sequentially. Figure S20A is the 10 µm thick slice, and Figure S20B is the 20 µm thick slice. The green circle in both images shows the gut area. The scale bar represents 250 µm.

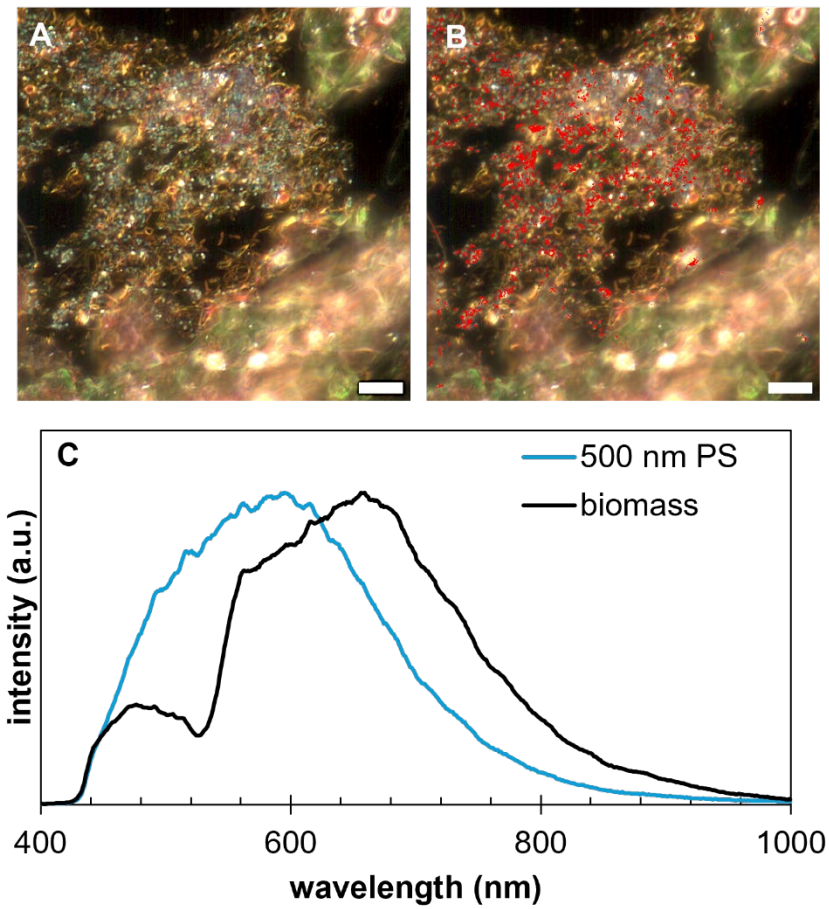

Figure S21. The second replicate of detecting ingested 500 nm PS at an exposure concentration of 0.01 ppm in *D. magna*. Histological slices were stained with 25% H&E stain. Figure S21A is the darkfield image acquired on the EDF-HSI microscope. Figure S21B is the corresponding Spectral Angle Mapping image, which shows the detection of PS particles in red. In Figure S21C, the blue curve is the average normalized spectrum of 50 pixels of plastic particles, and the black curve shows the average normalized spectrum of 50 pixels of biomass from Figure S21A. The peak wavelength for 500 nm PS and biomass is 595 nm and 659 nm, respectively. The brightness of Figures S21A and S21B has been increased by 40% to improve visualization. Figure S21A's sharpness was increased by 50%. Original images can be provided upon request.

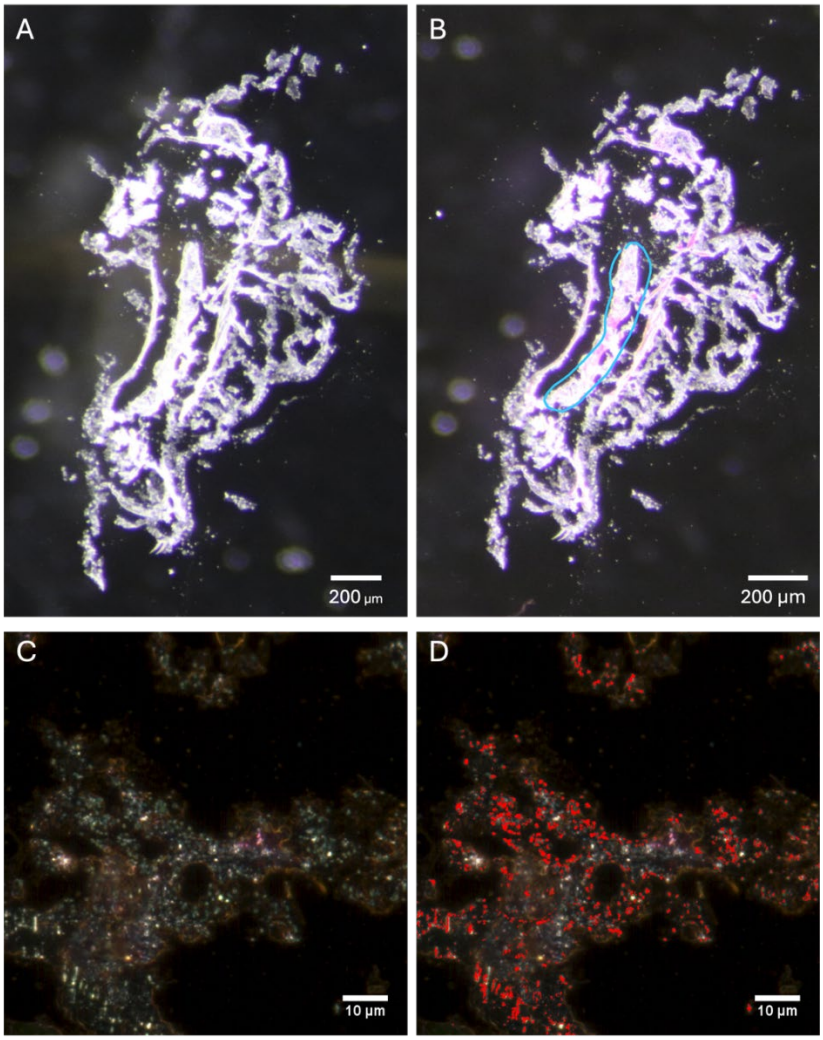

Figure S22. Third replicate of detecting 500 nm PS at 0.01 ppm within the gut of *D. magna.* Figure S22A is the darkfield image of a histological slice of the *D. magna* before staining. Figure S22B is the darkfield image of a histological slice of the *D. magna* after staining. The gut region is outlined in blue. Figure S22C was acquired using EDF-HSI and is the darkfield image of an area in the gut. Figure S22D is the corresponding mapped image, where 500 nm PS particles have been detected in red.

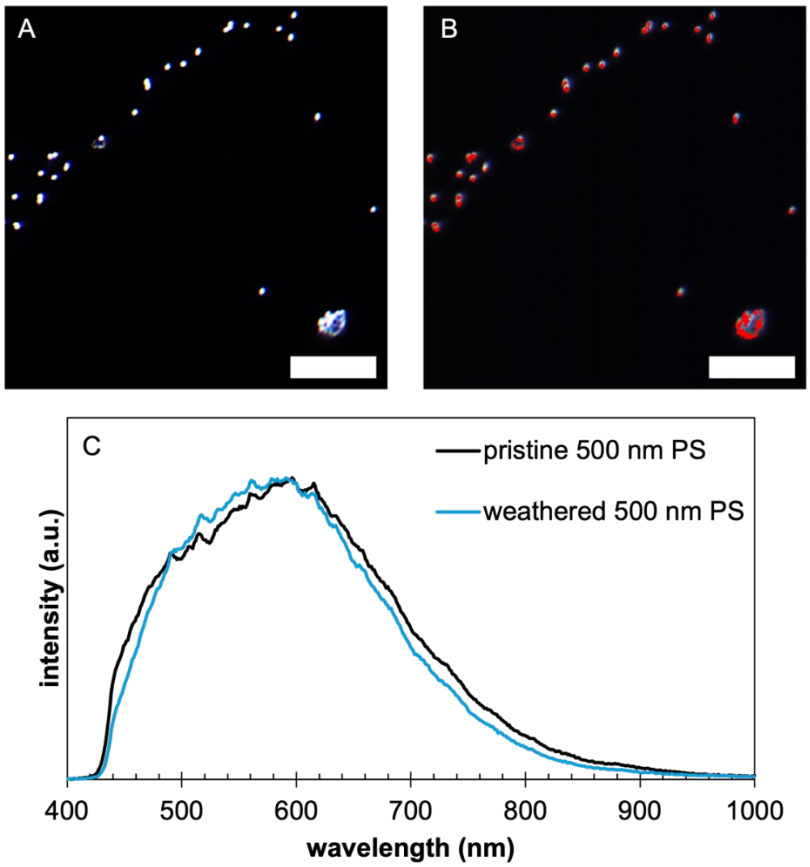

Figure S23. Detection of UV-weathered 500 nm PS. Figure S23A is the darkfield image of 500 nm PS particles that have been UV-weathered for 2 months. Figure S23B is the corresponding hyperspectral image, where the particles are detected in red. In Figure S23C, the blue curve is the average normalized spectrum of 50 pixels of UV-weathered 500 nm PS particles from Figure S23A, and the black curve shows the average normalized spectrum of 50 pixels of pristine 500 nm PS particles. The peak wavelength for weathered and pristine 500 nm PS is 591 nm and 596 nm, respectively. The brightness and contrast of Figure S23A have been increased by 40% and the sharpness was increased by 50% to improve visualization. Original images can be provided upon request.

Table S3. Comparing EDF-HSI with other microplastic and nanoplastic characterization tools.

	Detection limit	Sensitivity	Spatial preservation	Cost
EDF-HSI	~100 nm in a controlled matrix (e.g. polymeric suspended in DI or ultra-pure water), whereas this study reports 500 nm as the detection limit in a biological matrix.[2]	single particle acquisition is possible, resulting in detection of microplastics and nanoplastics at lower concentrations[3]	preserves organism structure on tissue sections,[4] or cells	~150,000 USD[5]
O-PTIR	reported detection limit is 500 nm;[6] however, in complex biological matrices, biomass interference can result in noisier signals. Thus, 1-2 µm particles results in better signal to noise ratio.[1]	single particle acquisition is possible, provided particles are larger than the detection limit. Possible to detect and identify microplastics at low concentrations.[1]	preserves sample integrity and requires minimal sample preparation[7]	>500,000 USD[8]
µRaman	typical resolution is ~1 µm;[9] advancements are being made for sub-micron detection[10, 11]	bulk sample analysis is the most common method, but single particle acquisition is also possible.[12]	requires some sample preparation, such as mounting on suitable substrates or tissue digestions.[9, 13]	~80,000 to 120,000 USD[14]
conventional HSI	used to characterize larger microplastics (>100 µm).[15-18]	single point acquisition is common, allowing for analysis of single particles larger than the detection limit.[15]	often requires dissections or digestions, resulting in a loss of spatial preservation.[19]	~40,000 to 200,000 USD[20]

References

(1) Macairan, J.-R.; Saherwala, A.; Li, F.; Monteil-Rivera, F.; Tufenkji, N. Label-Free Identification and Imaging of Microplastic and Nanoplastic Biouptake Using Optical Photothermal Infrared Microspectroscopy. *Environmental Science & Technology* **2025**. DOI: 10.1021/acs.est.4c14367.

(2) Nigamatzyanova, L.; Fakhrullin, R. Dark-field hyperspectral microscopy for label-free microplastics and nanoplastics detection and identification in vivo: A Caenorhabditis elegans study. *Environmental Pollution* **2021**, *271*, 116337. DOI: https://doi.org/10.1016/j.envpol.2020.116337.

(3) Fakhrullin, R.; Nigamatzyanova, L.; Fakhrullina, G. Dark-field/hyperspectral microscopy for detecting nanoscale particles in environmental nanotoxicology research. *Science of The Total Environment* **2021**, *772*, 145478. DOI: https://doi.org/10.1016/j.scitotenv.2021.145478.

(4) Kryuchkova, M. A.; Ishmukhametov, I. R.; Frank, Y. A.; Simakova, A. V.; Yartsev, V. V.; Nadueva, D. A.; Varenitsina, A. A.; Andreeva, Y. V.; Fakhrullin, R. F. Fluorescence-Free Tracking of Polystyrene Microplastics in Mosquito Larvae Using Dark-Field Hyperspectral Microscopy. *Colloid Journal* **2024**, *86* (3), 466-475. DOI: 10.1134/S1061933X24600167.

(5) Gosavi, D.; Cheatham, B.; Sztuba-Solinska, J. Label-Free Detection of Human Coronaviruses in Infected Cells Using Enhanced Darkfield Hyperspectral Microscopy (EDHM). *J Imaging* **2022**, *8* (2). DOI: 10.3390/jimaging8020024 From NLM.

(6) Prater, C. B.; Kansiz, M.; Cheng, J.-X. A tutorial on optical photothermal infrared (O-PTIR) microscopy. *APL Photonics* **2024**, *9* (9). DOI: 10.1063/5.0219983 (acccessed 1/11/2026).

(7) Gruber, E. S.; Karl, V.; Duswald, K.; Bhamidipalli, M. S.; Schlederer, M.; Limberger, T.; Kopatz, V.; Teleky, B.; Kenner, L.; Brandstetter, M. Method for label-free & non-destructive detection of microplastics in human formalin-fixed paraffin-embedded tissue sections. *Scientific Reports* **2025**, *15* (1), 42637. DOI: 10.1038/s41598-025-26751-1.

(8) Xie, J.; Gowen, A.; Xu, W.; Xu, J. Analysing micro- and nanoplastics with cutting-edge infrared spectroscopy techniques: a critical review. *Analytical Methods* **2024**, *16* (15), 2177-2197, 10.1039/D3AY01808C. DOI: 10.1039/D3AY01808C.

(9) Käppler, A.; Fischer, D.; Oberbeckmann, S.; Schernewski, G.; Labrenz, M.; Eichhorn, K.-J.; Voit, B. Analysis of environmental microplastics by vibrational microspectroscopy: FTIR, Raman or both? *Analytical and Bioanalytical Chemistry* **2016**, *408* (29), 8377-8391. DOI: 10.1007/s00216-016-9956-3.

(10) Xu, G.; Cheng, H.; Jones, R.; Feng, Y.; Gong, K.; Li, K.; Fang, X.; Tahir, M. A.; Valev, V. K.; Zhang, L. Surface-Enhanced Raman Spectroscopy Facilitates the Detection of Microplastics <1 μm in the Environment. *Environmental Science & Technology* **2020**, *54* (24), 15594-15603. DOI: 10.1021/acs.est.0c02317.

(11) Xie, L.; Gong, K.; Liu, Y.; Zhang, L. Strategies and Challenges of Identifying Nanoplastics in Environment by Surface-Enhanced Raman Spectroscopy. *Environmental Science & Technology* **2023**, *57* (1), 25-43. DOI: 10.1021/acs.est.2c07416.

(12) Anger, P. M.; von der Esch, E.; Baumann, T.; Elsner, M.; Niessner, R.; Ivleva, N. P. Raman microspectroscopy as a tool for microplastic particle analysis. *TrAC Trends in Analytical Chemistry* **2018**, *109*, 214-226. DOI: https://doi.org/10.1016/j.trac.2018.10.010.

(13) Araujo, C. F.; Nolasco, M. M.; Ribeiro, A. M. P.; Ribeiro-Claro, P. J. A. Identification of microplastics using Raman spectroscopy: Latest developments and future prospects. *Water Research* **2018**, *142*, 426-440. DOI: https://doi.org/10.1016/j.watres.2018.05.060.

(14) Services, B. T. *Confocal Raman Microscope Price: What You Need to Know Before Investing*. https://barnett-technical.com/confocal-raman-microscope-price-what-you-need-to-know-before-investing/#:~:text=Confocal%20Raman%20Microscopy%20is%20one%20of%20the,researchers%2C%20lab%20managers%2C%20and%20procurement%20teams%20alike: (accessed.
(15) Faltynkova, A.; Johnsen, G.; Wagner, M. Hyperspectral imaging as an emerging tool to analyze microplastics: A systematic review and recommendations for future development. *Microplastics and Nanoplastics* **2021**, *1* (1), 13. DOI: 10.1186/s43591-021-00014-y.
(16) Zhu, C.; Kanaya, Y.; Nakajima, R.; Tsuchiya, M.; Nomaki, H.; Kitahashi, T.; Fujikura, K. Characterization of microplastics on filter substrates based on hyperspectral imaging: Laboratory assessments. *Environmental Pollution* **2020**, *263*, 114296.
(17) Vidal, C.; Pasquini, C. A comprehensive and fast microplastics identification based on near-infrared hyperspectral imaging (HSI-NIR) and chemometrics. *Environmental pollution* **2021**, *285*, 117251.
(18) Gebejes, A.; Hrovat, B.; Semenov, D.; Kanyathare, B.; Itkonen, T.; Keinänen, M.; Koistinen, A.; Peiponen, K. E.; Roussey, M. Hyperspectral imaging for identification of irregular-shaped microplastics in water. *Sci Total Environ* **2024**, *944*, 173811. DOI: 10.1016/j.scitotenv.2024.173811 From NLM.
(19) Zhang, Y.; Wang, X.; Shan, J.; Zhao, J.; Zhang, W.; Liu, L.; Wu, F. Hyperspectral Imaging Based Method for Rapid Detection of Microplastics in the Intestinal Tracts of Fish. *Environmental Science & Technology* **2019**, *53* (9), 5151-5158. DOI: 10.1021/acs.est.8b07321.
(20) Stuart, M. B.; Stanger, L. R.; Hobbs, M. J.; Pering, T. D.; Thio, D.; McGonigle, A. J. S.; Willmott, J. R. Low-Cost Hyperspectral Imaging System: Design and Testing for Laboratory-Based Environmental Applications. *Sensors (Basel)* **2020**, *20* (11). DOI: 10.3390/s20113293 From NLM.